Supporting information

Using Paramagnetism to Slow Down Nuclear Relaxation in Protein NMR

Henry W. Orton, Ilya Kuprov, Choy-Theng Loh, Gottfried Otting

Contents

1. ^{15}N cross-correlated relaxation calculations

The equilibrium magnetization of the electron can be described using the magnetic susceptibility tensor χ,[1] which is anisotropic for most paramagnetic lanthanide ions.[2] Using a coordinate system with the paramagnetic centre located at its origin, the dipolar shielding tensor $\boldsymbol{\sigma}_{DS}$ at the nuclear site $\vec{r}$ can be calculated as[3]

$$\sigma_{DS} = \frac{1}{4\pi}\left[3\frac{\vec{r}\times\vec{r}}{r^5} - \frac{1}{r^3}\right]\cdot\chi \qquad (1)$$

The trace of the $\boldsymbol{\sigma}_{DS}$ tensor is the pseudocontact shift; it does not contribute to relaxation and must be subtracted to retain only the anisotropic component $\boldsymbol{\sigma}_{DS}^{aniso}$. The magnitude of this anisotropy that enters relaxation theory equations is then captured by the following quantity:[4]

$$\Delta_{DS}^2 = \sigma_x^2 + \sigma_y^2 + \sigma_z^2 - \sigma_x\sigma_y - \sigma_x\sigma_z - \sigma_y\sigma_z \qquad (2)$$

where σ_x, σ_y and σ_z denote the eigenvalues of the traceless tensor $\boldsymbol{\sigma}_{DS}^{aniso}$. The Curie spin relaxation contributions to the longitudinal and the transverse relaxation rates can then be calculated by applying the standard CSA relaxation theory.[5] When the presence of diamagnetic CSA is not taken into account, the Curie spin relaxation rates are

$$R_1 = \frac{2}{15}\Delta_{DS}^2\omega^2\left[\frac{\tau}{1+\omega^2\tau^2}\right] \quad (3)$$

$$R_2 = \frac{1}{45}\Delta_{DS}^2\omega^2\left[4\tau + \frac{3\tau}{1+\omega^2\tau^2}\right] \quad (4)$$

where ω denotes the nuclear Larmor frequency and τ is the rotational correlation time.

When CSA is taken into account, the corresponding tensor is added algebraically to $\boldsymbol{\sigma}_{DS}^{aniso}$. When the result is inserted into the standard CSA relaxation theory, this automatically takes into account the presence of CSA-DSA cross-correlation. If we denote the resulting tensor $\boldsymbol{\sigma}_{eff}$, its magnitude term within Bloch-Redfield-Wangsness relaxation theory expressions is identical to Equation (2):

$$\Delta_{eff}^2 = \sigma_x^2 + \sigma_y^2 + \sigma_z^2 - \sigma_x\sigma_y - \sigma_x\sigma_z - \sigma_y\sigma_z \quad (5)$$

where σ_x, σ_y and σ_z are now the eigenvalues of $\boldsymbol{\sigma}_{eff}$. To isolate the PRE, which now includes the cross-correlation effect, we subtract the diamagnetic CSA component:

$$\Delta_{PRE}^2 = \Delta_{eff}^2 - \Delta_{CSA}^2 \quad (6)$$

Multiple other relaxation mechanisms are present in the system. Importantly, the contribution from Solomon relaxation is negligible compared with Curie spin relaxation.[6] Other diamagnetic relaxation mechanisms are accounted for by subtracting the experimental relaxation rates measured for the diamagnetic reference, CbCaY. Equation (6) thus captures the PRE in its entirety.

The magnetic susceptibility tensor of the paramagnetic centre was calculated as $\boldsymbol{\chi} = \Delta\boldsymbol{\chi} + \boldsymbol{\chi}_{iso}$, using the $\Delta\boldsymbol{\chi}$ tensor determined from the PCS measurements. The isotropic part was calculated as

$$\boldsymbol{\chi}_{iso} = \frac{\mu_0\mu_B^2 g^2 J(J+1)}{3kT}\mathbf{1} \quad (7)$$

where μ_0 is the magnetic permeability of vacuum, μ_B is the Bohr magneton, k is the Boltzmann constant, T the absolute temperature, g the Landé g-factor, $\mathbf{1}$ is a 3×3 unit matrix, and J the total angular momentum quantum number for the given lanthanide (Tm^{3+} or Tb^{3+}; see the table in Ref. 2).

Having determined the $\boldsymbol{\chi}$ tensor of the paramagnetic centre in this way, the dipolar shift anisotropy effective at each backbone ^{15}N position was calculated using the crystal structure (PDB

ID: 4ICB[7]). The average CSA tensor reported for ubiquitin ^{15}N-spins (eigenvalues of -62.8, -45.7, and 108.5 ppm)[8] was then superimposed at each ^{15}N position and the cross-correlated PRE was calculated using Equation 5 and 6 and, subsequently, Equations 3 and 4. A rotational correlation time of τ = 4.25 ns was used for the spectral density.[9]

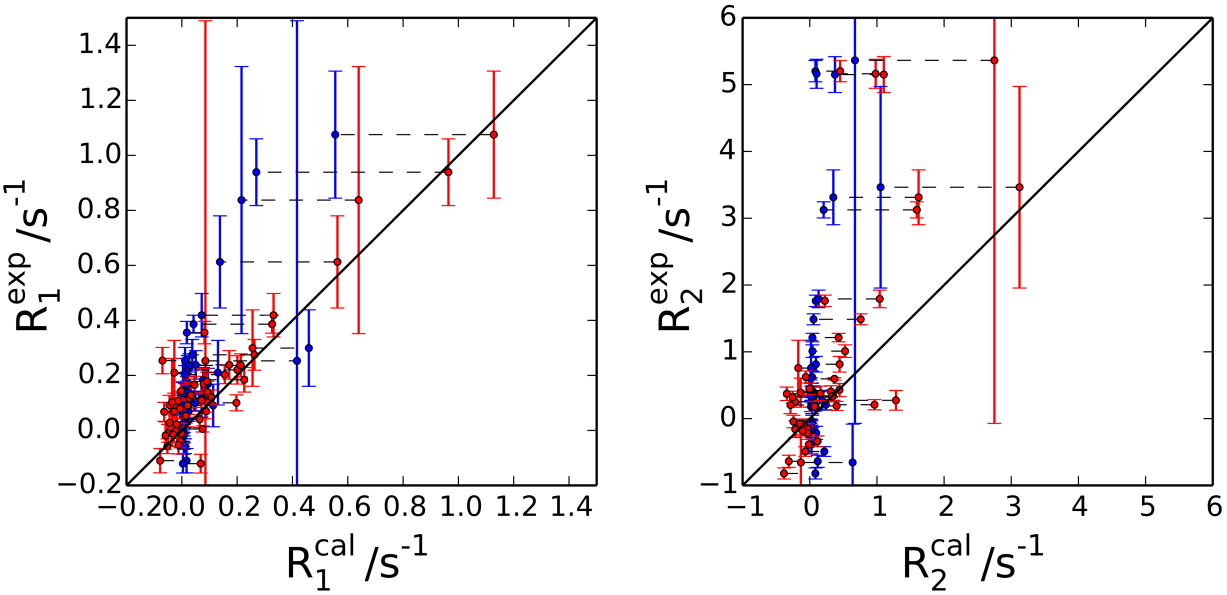

Figure S1. Experimental R_1(^{15}N) and R_2(^{15}N) PREs in calbindin D_{9k} *versus* predictions made by considering only Curie spin relaxation (blue points), and by including CSA-DSA cross-correlation (red points, this work). Left panel: same as Figure 2a of the main text, except that the plot captures the full data range. Right panel: same as Figure 2c of the main text, except showing the full data range.

2. Estimate of electron-nuclear distance for maximum negative PRE

Partial compensation of a CSA tensor by a DSA tensor (corresponding to a negative PRE) can occur at any distance from the paramagnetic center, except when the distance is so short that the CSA relaxation mechanism is overwhelmed by the Curie spin relaxation mechanism. Minimal and optimal distances for negative PREs can be estimated easily when the χ tensor is assumed to be isotropic and the CSA tensor to be axially symmetric. In this case, the DSA tensor is also axially symmetric and Δ_{eff} can be described in terms of the second degree Legendre polynomial P_2 and the angle θ between the principal axes of the DSA and CSA tensors.[6]

$$\Delta_{\mathrm{eff}}^2 = \Delta_{\mathrm{CSA}}^2 + \Delta_{\mathrm{DSA}}^2 - 2P_2(\cos\theta)\Delta_{\mathrm{CSA}}\Delta_{\mathrm{DSA}} \quad (8)$$

This function reaches its minimum value for θ = 90°, when

$$\Delta_{\text{eff}}^2 = \Delta_{\text{CSA}}^2 + \Delta_{\text{DSA}}^2 - 2\Delta_{\text{CSA}}\Delta_{\text{DSA}} \quad (9)$$

and becomes zero (corresponding to complete mutual cancellation of the two relaxation mechanisms) when $\Delta_{\text{CSA}} = \Delta_{\text{DSA}}$; this corresponds to the maximum of the paramagnetic narrowing. The dipolar shift anisotropy for a spin with an isotropic magnetic susceptibility tensor is[6]

$$\Delta_{\text{DSA}} = \frac{3}{4\pi}\frac{\chi_{\text{iso}}}{r^3} \quad (10)$$

The distance at which the maximum negative PRE occurs can then be estimated as

$$r = \sqrt[3]{\frac{3}{4\pi}\frac{\chi_{\text{iso}}}{\Delta_{\text{CSA}}}} \quad (11)$$

Negative PRE corresponds to $\Delta_{\text{eff}} < \Delta_{\text{CSA}}$, which is the same as $\Delta_{\text{DSA}} < 2\Delta_{\text{CSA}}$. Therefore, the minimum distance for a negative PRE may be estimated as

$$r > \sqrt[3]{\frac{3}{4\pi}\frac{\chi_{\text{iso}}}{2\Delta_{\text{CSA}}}} \quad (12)$$

Table S1. Lanthanide-^{15}N distance estimates for negative PREs of backbone ^{15}N spins.[a]

Lanthanide	***r*** / Å for max. paramagnetic narrowing	Min. ***r*** / Å for PRE < 0
Tm^{3+}	9.0	7.2
Tb^{3+}	10.7	8.5

[a] The calculations are for a ^{1}H NMR frequency of 600 MHz and assume an isotropic χ tensor (determined by Equation 7 using the parameters of the table in Ref. 3) and axially symmetric CSA tensors for backbone ^{15}N (eigenvalues of –54.25, –54.25, and 108.5 ppm). Distances of maximum paramagnetic narrowing were estimated using Equation 11. Minimum distances for observable negative PREs were estimated using Equation 12.

3. Protein sample preparation

Uniformly ^{15}N-labeled calbindin D_{9k} double mutant P43M/N56D was expressed in *E. coli* as a fusion protein with a His_6-tagged ubiquitin molecule at the N-terminus, using a high-cell density protocol.[10] Construction of the fusion protein and purification followed the strategy by Catanzariti et al.[11] The fusion protein was purified by a Ni-NTA affinity column and subsequently treated with 0.05 mole equivalents of His_6-tagged deubiquitinase enzyme to cleave off the ubiquitin. A second purification by Ni-NTA affinity chromatography yielded pure calbindin D_{9k} as the di-calcium complex (CbCaCa) in the flowthrough. Incubation for 30 minutes with 50 equivalents of DTPA produced apo-calbindin D_{9k} (Cb--). The solution was titrated with 1 equivalent of a lanthanide salt, $LnCl_3$, to form a 1:1 complex (Cb-Ln), after which a single equivalent of $CaCl_2$ was added to fill the vacant calcium binding site, giving (CbLnCa). The total yield of purified protein was about 10 mg per litre cell culture.

4. NMR measurements

All NMR measurements were conducted at 298 K with 0.25 mM solutions of CbTmCa, CbTbCa or CbYCa at pH 6.5 in a buffer containing 20 mM MES and 20 mM NaCl. The NMR data were recorded on Bruker Avance 800 MHz or 600 MHz NMR spectrometers equipped with TCI cryoprobes. The ^{1}H PCSs of backbone amides were measured by [^{15}N,^{1}H]-HSQC spectra and used to calculate the $\Delta\chi$ tensors using the program Numbat.[12] R_1(^{15}N) relaxation measurements were conducted on the 800 MHz NMR spectrometer in an interleaved manner using the pulse sequence of Figure S2 with relaxation delays of 10, 50, 100, 150, 250, 400, 600, 800, 1100 and 1500 ms.

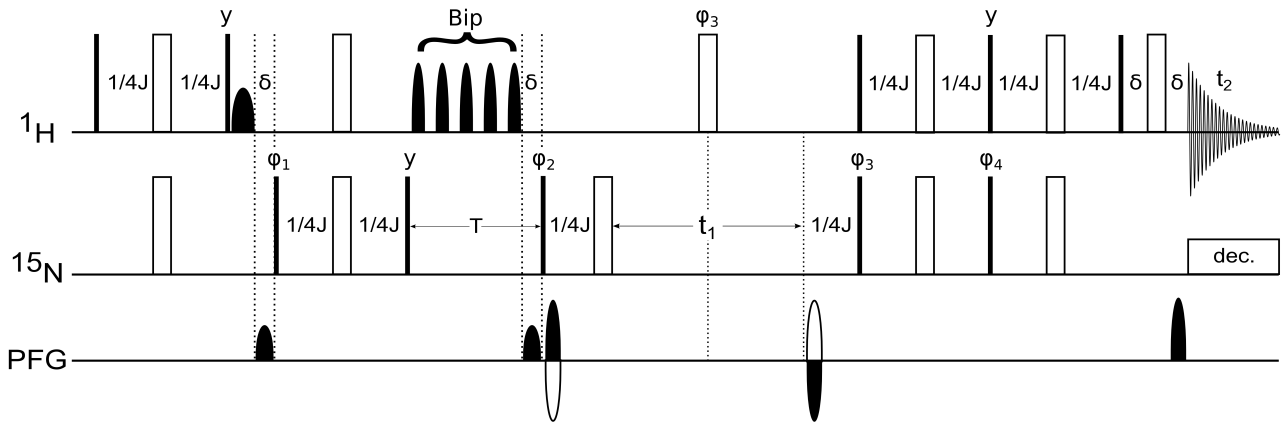

Figure S2. Pulse sequence used for the R_1(^{15}N) relaxation measurements. The pulse sequence corresponds to the Bruker standard pulse program hsqct1etf3gpsi3d.2. Sensitivity enhancement by the echo - anti-echo scheme was employed. Filled and open bars indicate 90° and 180° pulses, respectively. The shaped 90^{o} pulse on ^{1}H after the first INEPT achieves water flip-back. J was set to a ^{15}N-^{1}H coupling constant of 90 Hz. Bip pulses[13] were applied every 10 ms with alternating phase (x,-x) for the duration of the relaxation delay T to suppress the cross-correlation effect between dipolar and CSA relaxation. All pulses have phase x unless indicated otherwise. Phase cycle: φ_1 = (x,x,x,x,-x,-x,-x,-x), φ_2 = (y,-y), φ_3 = (x,x,-x,-x) , φ_4 = (-y,-y,y,y), receiver = (x,-x,-x,x,-x,x,x,-x). GARP decoupling was used during acquisition.

$R_2(^{15}N)$ relaxation measurements were conducted on the 600 MHz NMR spectrometer in the same interleaved manner, using the pulse sequence of Figure S3 with relaxation delays of 4, 50, 100, 200, 400 and 600 ms. The relaxation rate constants were determined by non-linear least squares regression, and the uncertainties were estimated by Monte-Carlo simulation, sourcing noise from the spectra.

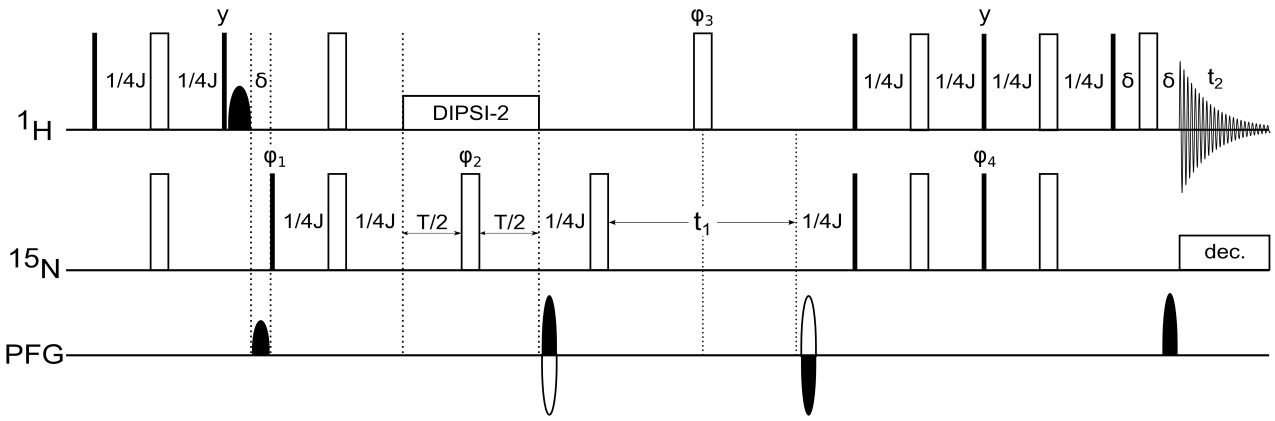

Figure S3. Pulse program used for the $R_2(^{15}N)$ relaxation measurements. The pulse sequence was modified from the Bruker standard pulse program hsqct2etf3gpsi3d by replacing the CPMG element on ^{15}N during the relaxation delay T by DIPSI-2 decoupling on ^{1}H to suppress the cross-correlation effect between dipolar and CSA relaxation. Filled and open bars indicate 90° and 180° pulses, respectively. The shaped 90° pulse on ^{1}H achieves water flip-back. J was set to a ^{15}N-^{1}H coupling constant of 90 Hz. All pulses have phase x unless indicated otherwise. Phase cycles are given by φ_1 = (x,-x), φ_2 = (x,x,x,x,y,y,y,y,-y,-y,-y,-y,-x,-x,-x,-x), φ_3 = (x,x,-x,-x), φ_4 = (-y,-y,y,y), receiver = (x,-x,-x,x,-x,x,x,-x). GARP decoupling was used during acquisition.

Table S2. Chemical shifts of backbone amides of CbCaY and PCSs for CbCaTm and CbCaTb

Residue Number	Residue Type	Y(H)/ppm	Y(N)/ppm	Tm(H) PCS/ppm	Tm(N) PCS/ppm	Tb(H) PCS/ppm	Tb(N) PCS/ppm
2	S	9.163	120.29	-0.244	-0.23	0.394	0.38
3	P	-	-	-	-	-	-
4	E	8.888	118.03	-0.557	-0.64	0.981	1.10
5	E	8.121	122.33	-0.530	-0.59	0.829	0.89
6	L	8.561	120.47	-0.615	-0.67	0.930	0.98
7	K	8.287	121.22	-1.108	-1.28	1.680	1.89
8	G	7.888	105.40	-1.086	-1.23	1.460	1.60
9	I	8.105	122.96	-0.911	-0.95	1.038	1.03
10	F	8.466	120.42	-1.422	-1.45	1.569	1.47
11	E	8.536	115.36	-2.107	-2.25	2.354	2.33
12	K	7.761	119.17	-1.509	-1.59	1.249	1.21
13	Y	7.321	115.12	-1.113	-1.00	0.620	0.44
14	A	8.321	119.50	-1.926	-1.73	1.325	0.97
15	A	6.874	117.05	-	-	1.128	1.10
16	K	7.178	120.21	-1.008	-0.95	0.093	0.09
17	E	9.684	116.18	-0.674	-0.55	-0.468	-0.42
18	G	9.013	113.17	-0.305	-0.48	-0.720	-0.77
19	D	8.358	128.17	-1.802	-1.99	-1.200	-0.64
20	P	-	-	-	-	-	-
21	N	9.069	115.11	-	-	4.066	4.75
22	Q	7.258	114.47	-	-	-	-
23	L	9.638	125.51	-	-	-	-
24	S	10.162	122.36	1.362	2.97	-	-
25	K	8.835	122.21	7.561	7.23	-	-
26	E	8.056	117.35	3.467	3.40	-	-
27	E	7.811	120.30	2.516	2.17	-	-
28	L	8.780	119.41	3.718	2.94	-	-
29	K	8.431	120.04	3.002	2.69	-	-
30	L	7.664	118.50	1.528	1.41	-	-
31	L	8.196	124.32	1.151	0.94	-2.082	-1.74
32	L	8.811	120.04	1.475	1.24	-2.388	-2.05
33	Q	8.628	114.57	1.096	1.00	-1.687	-1.57
34	T	7.653	110.89	0.646	0.59	-1.108	-1.00
35	E	8.414	116.18	0.486	0.40	-0.924	-0.77
36	F	7.868	114.89	0.615	0.59	-1.093	-0.98
37	P	-	-	-	-	-	-
38	S	8.398	113.69	0.546	0.54	-0.884	-0.87
39	L	7.968	122.70	0.779	0.73	-1.242	-1.22
40	L	7.731	117.00	0.932	0.96	-1.419	-1.44

41	K	7.460	120.43	0.806	0.78	-1.199	-1.13
42	G	8.077	108.85	0.725	0.67	-1.052	-0.98
43	M	8.357	120.06	0.685	0.70	-0.989	-1.02
44	S	8.253	115.18	0.860	0.89	-1.219	-1.23
45	T	8.110	113.87	1.103	1.16	-1.453	-1.51
46	L	8.682	122.51	1.664	1.94	-1.980	-2.34
47	D	8.118	117.54	1.937	2.40	-1.984	-2.53
48	E	7.796	119.58	1.719	1.96	-1.980	-2.24
49	L	8.381	121.79	2.653	2.95	-	-
50	F	8.985	119.36	5.096	6.26	-	-
51	E	7.871	116.16	4.101	5.13	-	-
52	E	7.716	118.68	3.329	2.94	-	-
53	L	7.849	114.94	8.564	8.42	-	-
54	D	8.297	120.59	-	-	-	-
55	K	7.766	122.90	-	-	-	-
56	D	7.709	114.30	-	-	-	-
57	G	7.906	109.11	-	-	-	-
58	D	8.075	118.11	-	-	-	-
59	G	10.309	112.75	-	-	-	-
60	E	7.551	117.38	-	-	-	-
61	V	10.936	132.62	-	-	-	-
62	S	9.610	127.78	-	-	-	-
63	F	9.624	123.42	-	-	-	-
64	E	8.429	118.41	-	-	-	-
65	E	8.088	121.18	-	-	-	-
66	F	8.854	119.05	-	-	-	-
67	Q	7.637	115.90	-1.655	-0.71	4.431	2.11
68	V	7.120	118.06	1.329	1.14	-	-
69	L	7.121	120.27	1.856	1.80	-	-
70	V	7.096	117.32	0.648	0.78	-1.010	-1.35
71	K	7.501	118.20	0.564	0.49	-0.863	-0.74
72	K	7.383	117.02	0.820	0.74	-1.438	-1.33
73	I	7.484	114.41	0.635	0.64	-1.112	-1.14
74	S	7.811	116.97	0.361	0.30	-0.625	-0.51
75	Q	7.617	126.28	0.256	0.23	-0.443	-0.38

Table S3. ^{15}N PREs for CbCaTm and CbCaTb[a]

Residue Number	R_1^{exp}(Tm)	R_2^{exp}(Tm)	R_1^{exp}(Tb)	R_2^{exp}(Tb)
2	-0.038 (0.025)	-0.156 (0.081)	-0.003 (0.023)	-0.38 (0.16)
3	-	-	-	-
4	0.053 (0.027)	0.181 (0.076)	0.001 (0.021)	0.82 (0.18)
5	0.021 (0.031)	-0.081 (0.076)	-0.048 (0.025)	0.64 (0.24)
6	0.140 (0.034)	-0.39 (0.14)	0.041 (0.029)	0.65 (0.34)
7	0.039 (0.030)	0.403 (0.088)	0.027 (0.027)	1.01 (0.29)
8	0.028 (0.035)	0.252 (0.082)	-0.131 (0.026)	1.25 (0.19)
9	-0.010 (0.032)	-0.043 (0.093)	-0.151 (0.029)	0.18 (0.29)
10	0.079 (0.036)	-0.213 (0.098)	0.037 (0.039)	1.16 (0.45)
11	0.067 (0.034)	-0.638 (0.091)	-0.098 (0.036)	-
12	0.254 (0.048)	0.37 (0.10)	-0.070 (0.034)	0.71 (0.31)
13	-0.110 (0.044)	-0.821 (0.083)	-0.15 (0.04)	-0.02 (0.36)
14	0.107 (0.035)	-0.492 (0.073)	-0.012 (0.061)	2.1 (1.5)
15	-	-	-0.175 (0.031)	-0.24 (0.25)
16	0.356 (0.041)	0.190 (0.068)	0.115 (0.032)	1.01 (0.28)
17	0.087 (0.029)	-0.338 (0.079)	0.064 (0.032)	0.64 (0.33)
18	0.275 (0.056)	0.27 (0.15)	0.326 (0.077)	1.89 (0.82)
19	0.21 (0.12)	-0.66 (0.57)	-0.00 (0.52)	-
20	-	-	-	-
21	-	-	0.00 (0.96)	-
22	-	-	-	-
23	-	-	-	-
24	-	10 (33)	-	-
25	0.3 (1.2)	-	-	-
26	0.169 (0.057)	7.1 (0.4)	-	-
27	0.117 (0.069)	7.11 (0.41)	-	-
28	0.091 (0.077)	-	-	-
29	0.238 (0.052)	7.59 (0.25)	-	-
30	0.178 (0.034)	0.81 (0.12)	-	-
31	0.165 (0.032)	1.760 (0.086)	0.286 (0.043)	1.56 (0.23)
32	0.139 (0.039)	5.20 (0.16)	0.147 (0.036)	-0.48 (0.19)
33	0.121 (0.027)	1.010 (0.094)	0.077 (0.025)	-0.23 (0.22)
34	0.102 (0.036)	0.429 (0.098)	0.103 (0.035)	1.68 (0.39)
35	0.128 (0.046)	0.38 (0.11)	-0.056 (0.023)	0.02 (0.13)
36	-0.002 (0.028)	-0.180 (0.081)	-0.043 (0.026)	-0.33 (0.15)
37	-	-	-	-
38	0.069 (0.067)	0.39 (0.22)	-0.040 (0.036)	0.41 (0.29)
39	0.092 (0.036)	-0.16 (0.12)	-0.015 (0.022)	0.28 (0.17)
40	-0.053 (0.033)	0.62 (0.09)	-0.11 (0.02)	0.290 (0.092)

41	-0.016 (0.024)	-0.078 (0.065)	-0.022 (0.021)	0.48 (0.11)
42	-0.012 (0.036)	0.448 (0.085)	0.005 (0.021)	0.010 (0.096)
43	0.10 (0.16)	0.76 (0.42)	-0.04 (0.13)	1.4 (0.9)
44	-0.020 (0.050)	0.20 (0.13)	0.008 (0.041)	-0.06 (0.26)
45	-0.058 (0.027)	0.320 (0.090)	-0.001 (0.022)	0.64 (0.18)
46	0.220 (0.052)	5.16 (0.22)	0.196 (0.041)	1.50 (0.39)
47	0.386 (0.033)	3.12 (0.12)	0.407 (0.040)	2.29 (0.30)
48	0.100 (0.029)	0.208 (0.077)	0.486 (0.083)	0.72 (0.35)
49	0.184 (0.045)	5.15 (0.27)	-	-
50	0.94 (0.12)	11.6 (1.2)	-	-
51	1.08 (0.23)	11.3 (3.1)	-	-
52	0.30 (0.14)	8.9 (1.7)	-	-
53	-	-	-	-
54	-	-	-	-
55	-	-	-	-
56	-	-	-	-
57	-	-	-	-
58	-	-	-	-
59	-	-	-	-
60	-	-	-	-
61	-	-	-	-
62	-	-	-	-
63	-	-	-	-
64	-	-	-	-
65	-	-	-	-
66	-	-	-	-
67	0.84 (0.49)	3.5 (1.5)	-	-
68	0.61 (0.17)	5.4 (5.4)	-	-
69	0.419 (0.079)	3.31 (0.41)	-	-
70	0.237 (0.042)	1.79 (0.13)	0.51 (0.12)	1.8 (1.1)
71	0.203 (0.033)	1.490 (0.082)	0.272 (0.034)	1.82 (0.23)
72	0.069 (0.027)	1.210 (0.064)	0.069 (0.049)	0.57 (0.24)
73	0.110 (0.026)	0.341 (0.065)	0.109 (0.034)	0.45 (0.23)
74	-0.121 (0.034)	0.330 (0.079)	-0.088 (0.025)	0.79 (0.15)
75	0.005 (0.011)	0.596 (0.018)	0.0181 (0.0077)	0.030 (0.024)

[a] All values are given in s^{-1}. Uncertainties (given in brackets) were determined by a Monte-Carlo simulation, where the fitting to the data was repeated 500 times after randomly adding noise from the spectrum, taking the standard deviation of all fitted rates.

References

(1) Guéron, M. Nuclear Relaxation in Macromolecules by Paramagnetic Ions: a Novel Mechanism. *J. Magn. Reson*. **1975**, *19*, 58-66.

(2) Pintacuda, G.; John, M.; Su, X.-C.; Otting, G. NMR Structure Determination of Protein-Ligand Complexes by Lanthanide Labeling. *Acc. Chem. Res*. **2007**, *40*, 206-212.

(3) Vega, A. J.; Fiat, D. Nuclear Relaxation Processes of Paramagnetic Complexes. The Slow-Motion Case. *Mol. Phys.* **1976**, *31*, 347-355.

(4) Chalmers, K. H.; De Luca, E.; Hogg, N. H. M.; Kenwright, A. M.; Kuprov, I.; Parker, D.; Botta, M.; Wilson, J. I.; Blamire, A. M. Design Principles and Theory of Paramagnetic Fluorine-Labelled Lanthanide Complexes as Probes for ^{19}F Magnetic Resonance: A Proof-of-Concept Study. *Chem. Eur. J.* 2010, *16*, 134-148.

(5) Cavanagh, J; Fairbrother, W. J.; Palmer, A. G.; Rance, M.; Skelton, N. J. Protein NMR Spectroscopy. Elsevier Academic Press: Burlington, USA, 2007.

(6) Pintacuda, G.; Kaikkonen, A.; Otting, G. Modulation of the Distance Dependence of Paramagnetic Relaxation Enhancements by CSAxDSA Cross-Correlation. *J. Magn. Reson*. **2004**, *171*, 233-243.

(7) Svensson, L. A.; Thulin, E.; Forsén, S. Proline *cis-trans* Isomers in Calbindin D_{9k} Observed by X-Ray Crystallography. *J. Mol. Biol*. **1992**, *223*, 601–606.

(8) Cornilescu, G.; Bax, A. Measurement of Proton, Nitrogen, and Carbonyl Chemical Shielding Anisotropies in a Protein Dissolved in a Dilute Liquid Crystalline Phase. *J. Am. Chem. Soc*. **2000**, *122*, 10143-10154.

(9) Kördel, J.; Skelton, N. J.; Akke, M.; Palmer III, A. G.; Chazin, W. J. Backbone Dynamics of Calcium-Loaded Calbindin D_{9k} Studied by Two-Dimensional Proton-Detected ^{15}N NMR Spectroscopy. *Biochemistry* **1992**, *31*, 4856-4866.

(10) Sivashanmugam, A.; Murray, V.; Cui, C. X.; Zhang, Y. H.; Wang, J. J.; Li, Q. Practical Protocols for Production of Very High Yields of Recombinant Proteins Using *Escherichia coli*. *Protein Sci*. **2009**, *18*, 936–948.

(11) Catanzariti, A. M.; Soboleva, T. A.; Jans, D. A.; Board, P. G.; Baker, R. T. An Efficient System for High-Level Expression and Easy Purification of Authentic Recombinant Proteins. *Protein Sci*. **2004**, *13*, 1331-1339.

(12) Schmitz, C.; Stanton-Cook, M. J.; Su, X.-C.; Huber, T. Numbat: an Interactive Software Tool for Fitting $\Delta\chi$-Tensors to Molecular Coordinates Using Pseudocontact Shifts. *J. Biomol. NMR* **2008**, *41*, 179-189.

(13) Smith, M. A.; Hu, H.; Shaka, A. J. Improved Broadband Inversion Performance for NMR in Liquids. *J. Magn. Reson*. **2001**, 151, 269-283.